[CANCER RESEARCH 64, 4400–4404, July 1, 2004]

Advances in Brief

Peritumor Lymphatics Induced by Vascular Endothelial Growth Factor-C Exhibit Abnormal Function

Naohide Isaka, Timothy P. Padera, Jeroen Hagendoorn, Dai Fukumura, and Rakesh K. Jain

E. L. Steele Laboratory for Tumor Biology, Department of Radiation Oncology, Massachusetts General Hospital and Harvard Medical School, Boston, Massachusetts

Abstract

Vascular endothelial growth factor (VEGF)-C is known to induce hyperplasia in normal murine lymphatics and in peritumor lymphatics. Here, we examine the function of these hyperplastic peritumor lymphatics. Microlymphangiography of B16F10 melanomas growing in the murine dorsal skinfold chamber showed that the number of functional, draining lymphatics in the peritumor tissue of VEGF-C-overexpressing tumors was significantly greater than that in mock-transduced tumors (9.5 ± 1.0 *versus* 6.3 ± 0.4; $n = 6$; $P < 0.05$). Forty percent of functional lymphatics associated with VEGF-C-overexpressing tumors contained proliferating lymphatic endothelial cells. Surprisingly, these new, functional lymphatic vessels displayed a retrograde draining pattern, which indicates possible dysfunction of the intraluminal valves of these vessels.

Introduction

Vascular endothelial growth factor (VEGF)-C is an important player in lymphatic metastasis (1). The innate production and overexpression of VEGF-C in tumor models induces hyperplasia in peritumor lymphatics, yet how well these lymphatics function is not known (2–6). The effects of VEGF-C on the function of preexisting lymphatic vessels and the formation of new, functional lymphatics will have broad implications for antilymphangiogenic therapy and drug delivery to tumors (7). Unfortunately, there is a paucity of animal models that permit intravital observation of physiological and pathological lymphatic function (2). Current murine lymphangiogenesis models include implanted tumors in the tail (3, 6), a collagen implant in the tail (8), the cornea (9), and the ear (10). However, to date, none of these models have been used to observe the function and quality of hyperplastic peritumor lymphatics. Here we use, for the first time, the murine dorsal skinfold chamber (DSC) model (11) and microlymphangiography (3, 6) to measure the function of normal skin lymphatics and newly formed lymphatics around VEGF-C-overexpressing tumors.

Materials and Methods

Animals and Tumor Cells. The experiments were performed in severe combined immunodeficient (SCID) or C57BL/6 male mice (body weight $>$ 28 g) bred and maintained in our gnotobiotic animal colony at Massachusetts General Hospital. All procedures were carried out following the Public Health Service Policy on Humane Care of Laboratory Animals and approved by the Institutional Animal Care and Use Committee of Massachusetts General Hospital. VEGF-C-overexpressing (B16F10-VEGF-C) and mock-transduced (B16F10-MT) B16F10 melanoma cell lines were established and cultured as reported previously (12).

DSC Implantation. The preparation of the DSC has been described previously (Fig. 1*A*; Ref. 13). Briefly, mice were anesthetized (90 mg of ketamine HCl and 9 mg xylazine/kg body weight, s.c.), the dorsal skin was shaved and depilated, and two mirror-image titanium frames were mounted to fix the extended double layer of skin between the frames. One 15-mm-diameter layer of skin was excised, leaving the striated muscle, s.c. tissue, and epidermis of the opposite side intact. The tissue was covered with a glass coverslip mounted into the frame. For investigating lymphatics associated with tumors, a small piece (~1 mm in diameter) of B16F10-VEGF-C or B16F10-MT tumor was implanted into the center of chambers.

Lymphangiography. To identify the lymphatics in the DSC of SCID mice ($n = 8$), 1–2 μl of 4% Evan's blue dye ($M_r = 960$; Sigma) in PBS were intradermally injected into the caudal-medial site of the DSC from the back side using a 30-gauge needle. To prevent tissue and lymphatic destruction and obtain stable lymphatic network images, injections were performed with very low and stable pressure. To optimize the lymphangiography, we injected in various places in and around the DSC and found that caudal-medial injections were the most effective to obtain lymphatic network images in the DSC. After injection, mice were immediately immobilized and placed on a stage designed to stabilize the DSC under a stereomicroscope (Stemi 2000; Zeiss, Jena, Germany). Images were acquired by a digital camera (Cyber Shot; Sony, Tokyo, Japan) between 5 and 10 min after injection. Similarly, lymphangiography of tumor-associated lymphatics was performed using C57BL/6 mice from which the B16F10 murine melanoma cell line was derived. The following groups were investigated: no-tumor control group ($n = 6$); B16F10-MT group ($n = 6$); and B16F10-VEGF-C group ($n = 6$). When tumors reached 12 mm^2 surface area (between 5 and 16 days after implantation), 1–2 μl of Evan's blue dye were injected intradermally in the back side of the tumor using a 30-gauge needle, and images were taken as described above. The number of lymphatics draining from the injected area was counted. Retrograde lymphatics were categorized as functional lymphatics that impinged on the edge of the caudal half of the DSC window.

Multiphoton Laser Scanning Microscopy. The use of multiphoton laser scanning microscopy and tissue lymphangiography has been described previously (14, 15). For simultaneous visualization of blood and lymphatic vessels, mice were anesthetized as described above and received i.v. injection with 0.1 ml of M_r 2,000,000 tetramethyl-rhodamine-dextran (Molecular Probe, Eugene, OR) at a concentration of 10 mg/ml in PBS. Immediately thereafter, fluorescence microlymphangiography was performed by a slow, intradermal injection of 2 μl of M_r 2,000,000 FITC-dextran (Sigma, St. Louis, MO) at a concentration of 25 mg/ml in PBS, at the caudal-medial site of the DSC. After these injections, the animal was fixed to a metal plate designed to stabilize the chamber, and multiphoton laser scanning microscopy was performed to visualize the microvasculature and microlymphatics.

Immunohistochemistry of Lymphatics. Ten min before sacrifice, 1–2 μl of ferritin were slowly injected at the center of the back side of the tumor to identify functional lymphatics. The tumors and peritumor tissues were excised, fixed in 4% paraformaldehyde for 12 h, and embedded in paraffin. Sections (4-μm thick) were immunostained with monoclonal antibodies against proliferating cell nuclear antigen (DAKO, Carpinteria, CA) using the manufacturer's protocol. A 5% potassium ferrocyanide and 10% HCl solution was used to reveal the iron III component of ferritin according to published protocols (3). To confirm that ferritin-positive structures were lymphatics, immunostaining with Prox 1, a molecular lymphatic marker, was performed according to published protocols (16). To determine the presence of a smooth muscle layer

Received 3/1/04; accepted 4/19/04.

Grant support: NIH Bioengineering Research Partnership Grant R24-CA85140.

The costs of publication of this article were defrayed in part by the payment of page charges. This article must therefore be hereby marked *advertisement* in accordance with 18 U.S.C. Section 1734 solely to indicate this fact.

Note: Naohide Isaka is currently at Department of Surgery, Sakura Citizen Hospital, Chiba, Japan.

Requests for reprints: Rakesh K. Jain, Department of Radiation Oncology, Massachusetts General Hospital, 100 Blossom Street, Cox 734, Boston, MA 02114. Phone: (617) 726-4083; Fax: (617) 724-1819; E-mail: jain@steele.mgh.harvard.edu.

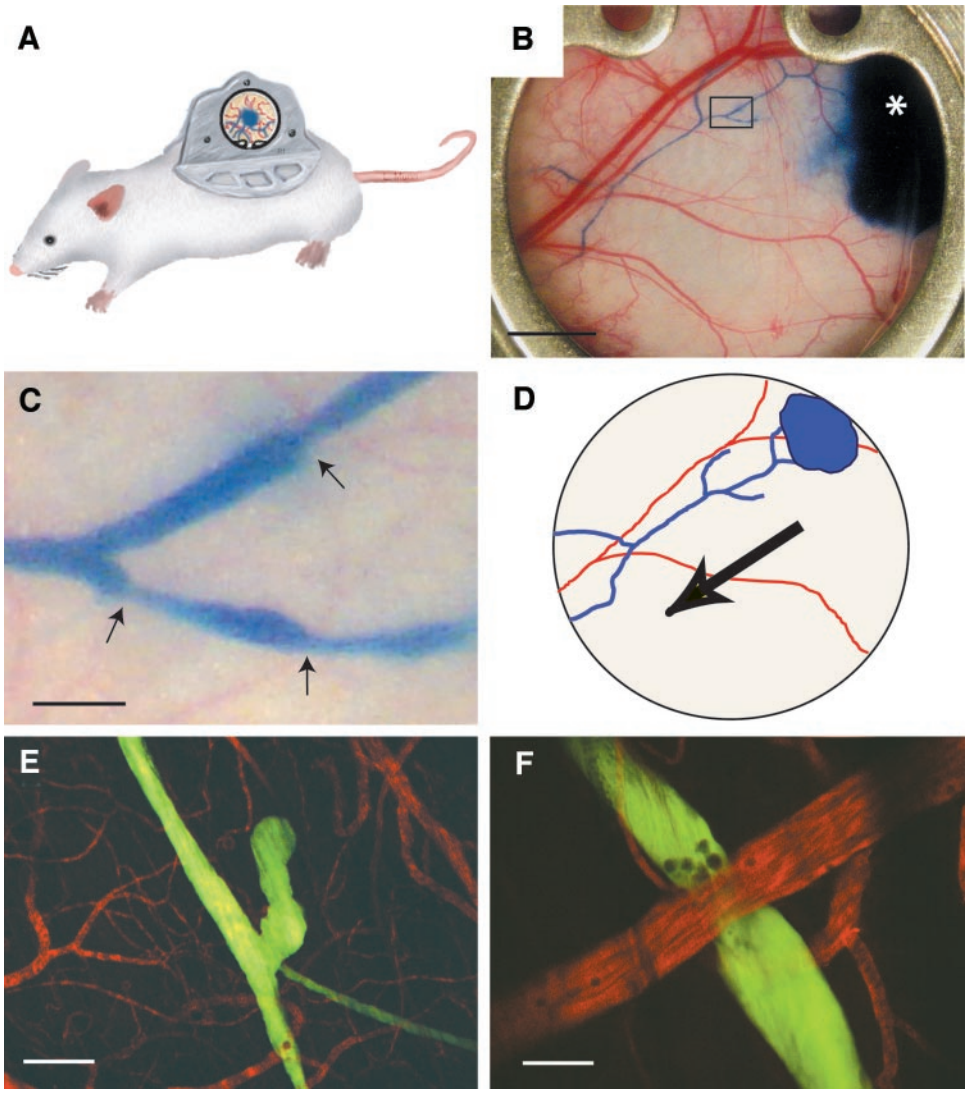

Fig. 1. Imaging lymphatics in the dorsal skinfold chamber. *A*, schematic image of the dorsal skin fold chamber. *B*, macroscopic images after Evan's blue dye injection at the caudal-medial site (*asterisk*) in the dorsal skinfold chamber. The *boxed area* is shown in *C*. *C*, lymphatic valves are located where there are diameter changes (*arrows*). *D*, schematic image of *B*. *Blue*, lymphatic vessels draining area of dye injection; *red*, blood vessels; *arrow*, direction of lymph flow (caudal-medial to cranial-lateral). *E* and *F*, representative images of multiphoton laser scanning microscopy. *Green*, lymphatics; *red*, blood vessels. *F*, several lymphocytes are seen in front of the lymphatic valve. *Scale bars*: 2 mm (*B*); 200 μm (*C*); 100 μm (*E*); and 50 μm (*F*).

around the lymphatics, α-smooth muscle actin immunostaining was performed according to published protocols (17).

Northern Blot Analysis. Northern blot analysis was performed using previously published methods (12). The murine VEGF-C cDNA probe was synthesized by PCR (primers: forward, 5′-CAAGGCTTTTGAAGGCAAAG-3′; reverse, 5′-TGCTGAGGTAACCTGTGCTG-3′).

Results

Functional Lymphangiography in the DSC Model. Lymphatic networks were apparent and distinct from blood vessels after Evan's blue dye injection in the DSC of SCID mice (Fig. 1*B*). The lymphangiography showed the characteristic lymphangion structure with periodic bulbous swelling between valves (Fig. 1*C*). Lymph flow occurred mainly from caudal-medial to cranial-lateral, making the caudal-medial injection site necessary (Fig. 1*D*). The dye-filled vessels in the DSC drained directly to lateral axillary lymph nodes and stained them blue (data not shown). We could perform lymphangiography successfully in seven of eight SCID mice, indicating the reproducibility in observing the lymphatic system in the DSC.

Functional Microlymphangiography using Multiphoton Laser Scanning Microscopy. We injected tetramethyl-rhodamine-dextran i.v. and FITC-dextran intradermally at the caudal-medial site within the DSC and obtained detailed images of lymphatics (*green*) and blood vessels (*red*; Fig. 1, *E* and *F*). FITC-dextran was almost completely retained within the lymphatics. We could easily distinguish lymphatics from blood vessels. The blind-ended initial lymphatics (around 70 μm in diameter) were larger than blood capillaries.

Lymphangiography of VEGF-C-Overexpressing Tumors Shows New, Functional Lymphatics in Peritumor Tissue. B16F10-MT and B16F10-VEGF-C tumors expressing nondetectable and high levels of VEGF-C, respectively (Fig. 2*A*), were grown in the DSC. Lymphangiography in the DSC in C57BL/6 mice without a tumor and in mice with B16F10-MT tumors was similar to that in SCID mice, with lymph flow in the caudal-medial to cranial-lateral directions (Fig. 2, *B*, *C*, *E*, and *F*). Lymphangiography in the DSC of mice with B16F10-VEGF-C tumors, however, showed a greater number of functional lymphatics in the peritumor tissue (Fig. 2, *D*, *G*, and *H*). α-Smooth muscle actin staining was absent in nearly all these peritumor lymphatics, and this confirmed that these were initial and not collecting lymphatics (data not shown). Surprisingly, the pattern of lymphatic flow around B16F10-VEGF-C tumors was different, with flow occurring in most directions away from the tumor, not only in the caudal-medial to cranial-lateral direction (Fig. 2, *D* and *G*). This alteration was quantified by a greater number of retrograde lymphatics impinging

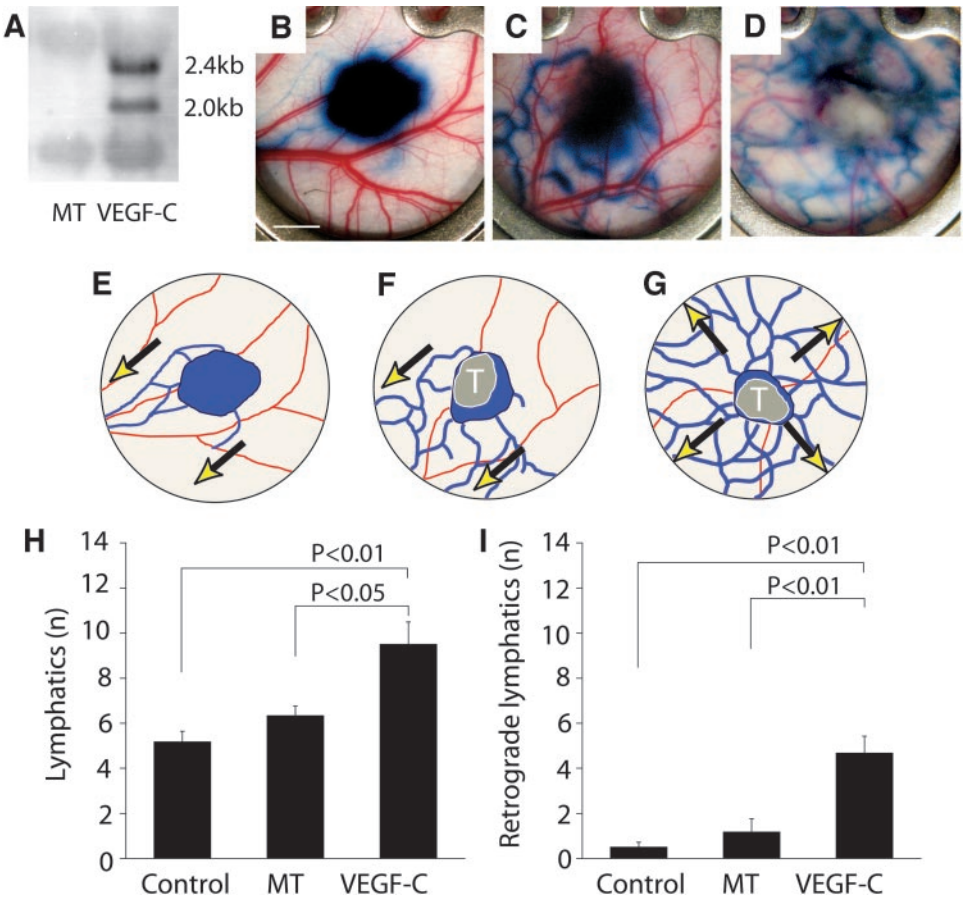

Fig. 2. Overexpression of vascular endothelial growth factor (VEGF)-C increases the number of functional, draining lymphatics in peritumor tissue. *A*, Northern blot analysis confirmed overexpression of VEGF-C. Endogenous VEGF-C expression was below the detection limit. *B*−*D*, lymphangiography in dorsal skinfold chamber (DSC) of no-tumor control (*B*), B16F10-MT tumor (*C*), and B16F10-VEGF-C tumor (*D*). Evan's blue dye was injected at the center area of the DSC (*B*) and at the peritumor tissue area (*C* and *D*) to identify functional lymphatics. *E*−*G*, schematic images of *B*−*D*, respectively. *Blue*, lymphatic vessels draining area of dye injection; *red*, blood vessels; *arrows*, direction of lymph flow. *H*, quantification of lymphatics draining from Evan's blue dye injection area. The mean and SE of the number of lymphatics counted are shown. B16F10-VEGF-C tumors (9.5 ± 1.0) showed a significantly increased number of functional, draining lymphatics compared with B16F10-MT tumors (6.3 ± 0.4) and no-tumor control (5.2 ± 0.5). *I*, quantification of retrograde lymphatics impinging on the caudal edge of the DSC. The mean and SE of the number of lymphatics counted are shown. B16F10-VEGF-C tumors (4.7 ± 0.8) showed a significantly increased number of lymphatics compared with B16F10-MT tumors (1.2 ± 0.6) and no-tumor control (0.5 ± 0.2). Data between groups were compared by unpaired *t* test. $n = 6$ in each group (*H* and *I*). *Scale bar*, 2.0 mm (*B*−*D*).

on the caudal edge of the DSC with B16F10-VEGF-C tumors (Fig. 2*I*). This implies that there may be dysfunction in the intraluminal valves of these vessels.

Cell Proliferation in Functional Lymphatic Vessels. To assess whether functional lymphatics resulted from lymphangiogenesis, ferritin lymphangiography and proliferating cell nuclear antigen immunohistochemistry were performed on sections of B16F10-VEGF-C tumors from the DSC. Open structures containing ferritin were found in the peritumor tissue, and a few were found in the tumor margin as well (within 100 μm on either side of the tumor edge; Fig. 3*A*). No functional lymphatics were observed inside of the tumor. Double staining for proliferating cell nuclear antigen and ferritin revealed that 40% of functional lymphatics associated with VEGF-C-overexpressing tumors contained proliferating lymphatic endothelial cells (Fig. 3, *B* and *C*). Double staining of ferritin and Prox 1 confirmed that ferritin-positive structures were functional lymphatics (Fig. 3*D*).

Discussion

Despite the recent discovery of lymphangiogenic factors such as VEGF-C and VEGF-D, many questions remain regarding the molecular mechanisms of lymphangiogenesis as well as lymphatic metastasis. Appropriate models and techniques that can reveal lymphatic function microscopically have been a challenge to develop (2, 11). The emergence of the DSC model as a tool to study the lymphatic system makes it possible to measure lymphatic diameters and branching patterns, to observe the initial lymphatics in which tumor cells may enter, to study intraluminal valves, to study macromolecular uptake by lymphatics, and to observe the interaction between tumor cells and lymphatics.

In concert with our previous findings (3, 6, 17), we found a lack of functional lymphatics in B16F10-VEGF-C or B16F10-MT tumors after intratumor injections of Evan's blue dye or ferritin. However, we could easily identify functional lymphatics in the tumor margin and peritumor tissue in these models. In agreement with published reports (18, 19), our study showed that an increased number of functional, draining lymphatics were associated with the VEGF-C-overexpressing tumors. Furthermore, we showed that the endothelial cells associated with nearly 40% of functional lymphatics were proliferating, suggesting that active lymphangiogenesis can occur in the peritumor tissue. Thus, VEGF-C-overexpressing tumors were capable of inducing the formation of new, functional lymphatics.

Besides the apparent increase in the number of lymphatics, the direction of flow also was altered by VEGF-C. Lymphatics induced by VEGF-C allowed retrograde flow, potentially because the intraluminal valves were unable to close properly and were thus unable to prevent lateral flow into side lymphatics (10, 20). This suggests that VEGF-C induces new but immature lymphatics. Similar to the maturation of VEGF-A-induced blood vessels (21), the maturation of VEGF-C-induced lymphatic vessels may require a constellation of molecules.

In conclusion, this study demonstrates that the DSC is a useful model to study the lymphatic system using intravital microscopy *in vivo*. Furthermore, VEGF-C produced by the tumor induced new, functional lymphatic vessels around the tumor, although the direction of lymph flow was altered. The formation of new yet functionally aberrant lymphatics by elevated VEGF-C levels calls for further research into the processes of lymphatic vessel maturation.

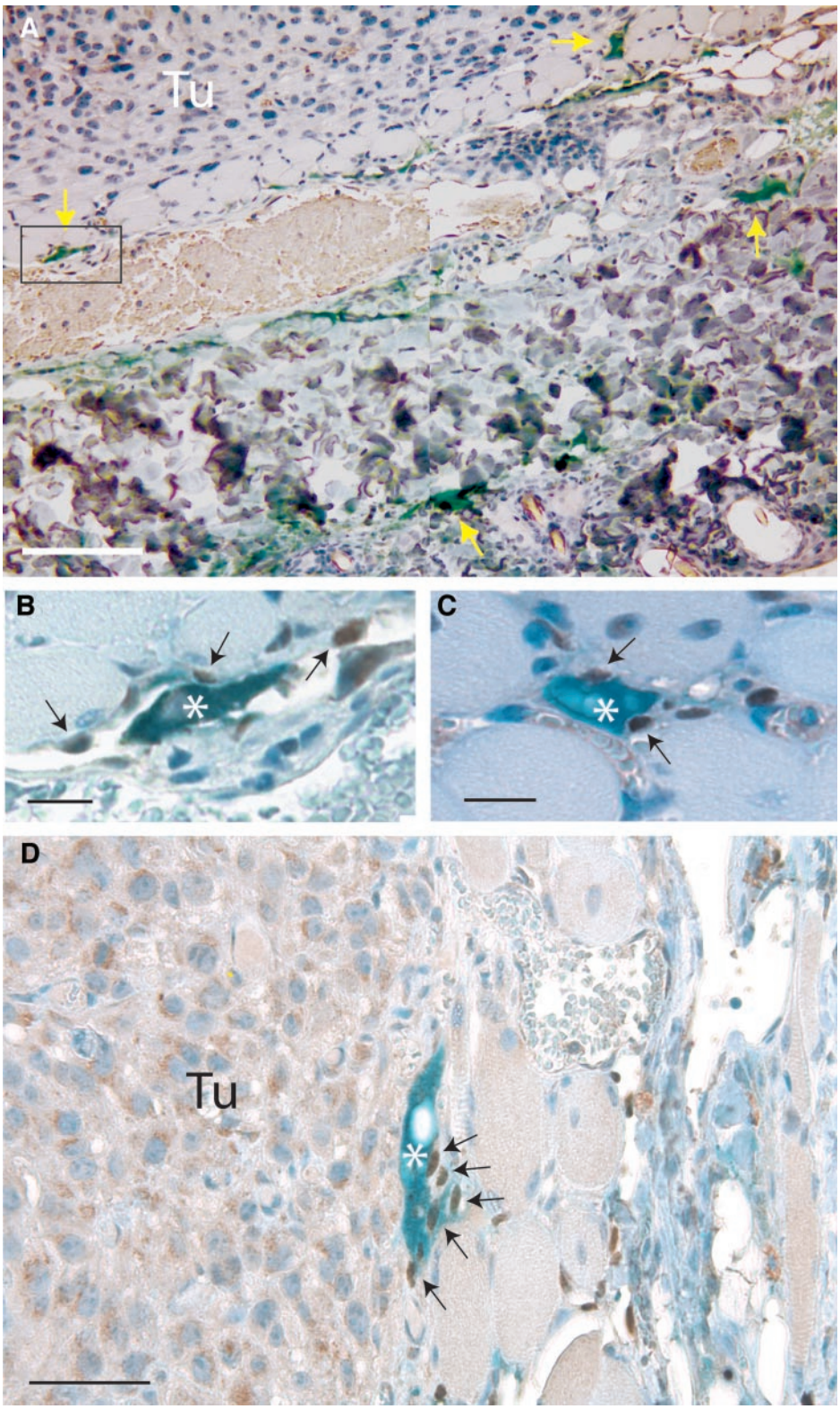

Fig. 3. Vascular endothelial growth factor C-overexpressing tumor induces peritumor lymphatic endothelial cell proliferation. *A*, immunohistochemistry for injected ferritin shows functional, draining lymphatics (*blue-green area, arrows*) only in the tumor margin and peritumor tissue. The *boxed area* is shown in a serial section in *B*. *B* and *C*, double staining for proliferating cell nuclear antigen and ferritin. Proliferating cell nuclear antigen-positive (*brown nuclei, arrows*) lymphatic endothelial cells are seen around the ferritin-filled functional lymphatics (*asterisk*). *D*, double staining for ferritin and Prox 1. Prox 1-positive (*brown nuclei, arrows*) lymphatic endothelial cells are seen around the ferritin-filled functional lymphatics (*asterisk*). Prox 1-positive cells also identify non-ferritin-filled lymphatics in peritumor tissue. *Tu*, tumor (*A* and *D*). *Scale bars*: 100 μm (*A*); 20 μm (*B and C*); and 50 μm (*D*).

Acknowledgments

We thank Dr. Stanislav I. Tomarev for the generous supply of Prox 1 antibody; Jessica B. Tooredman, Julia Kahn, Sylvie Roberge, and Carolyn J. Smith for outstanding technical assistance; Dr. Lance Munn for assistance with illustrations; Dr. Peigen Huang for helpful suggestions; and Dr. Mutsumi Nozue for support.

References

1. Alitalo K, Carmeliet P. Molecular mechanisms of lymphangiogenesis in health and disease. Cancer Cell 2002;1:219–27.
2. Jain RK, Fenton BT. Intratumoral lymphatic vessels: a case of mistaken identity or malfunction? J Natl Cancer Inst (Bethesda) 2002;94:417–21.
3. Leu AJ, Berk DA, Lymboussaki A, Alitalo K, Jain RK. Absence of functional lymphatics within a murine sarcoma: a molecular and functional evaluation. Cancer Res 2000;60:4324–7.

4. Mandriota SJ, Jussila L, Jeltsch M, et al. Vascular endothelial growth factor-C-mediated lymphangiogenesis promotes tumor metastasis. EMBO J 2001;20:672–82.
5. Skobe M, Hawighorst T, Jackson DG, et al. Induction of tumor lymphangiogenesis by VEGF-C promotes breast cancer metastasis. Nat Med 2001;7:192–5.
6. Padera TP, Kadambi A, di Tomaso E, et al. Lymphatic metastasis in the absence of functional intratumor lymphatics. Science (Wash DC) 2002;296:1883–6.
7. Jain RK, Padera TP. Prevention and treatment of lymphatic metastasis by antilymphangiogenic therapy. J Natl Cancer Inst (Bethesda) 2002;94:785–7.
8. Boardman KC, Swartz MA. Interstitial flow as a guide for lymphangiogenesis. Circ Res 2003;92:801–8.
9. Chang L, Kaipainen A, Folkman J. Lymphangiogenesis new mechanisms. Ann NY Acad Sci 2002;979:111–9.
10. Nagy JA, Vasile E, Feng D, et al. Vascular permeability factor/vascular endothelial growth factor induces lymphangiogenesis as well as angiogenesis. J Exp Med 2002; 196:1497–506.
11. Jain RK, Munn LL, Fukumura D. Dissecting tumor pathophysiology using intravital microscopy. Nat Rev Cancer 2002;2:266–76.
12. Kadambi A, Mouta Carreira C, Yun C, et al. Vascular endothelial growth factor (VEGF)-C differentially affects tumor vascular function and leukocyte recruitment: role of VEGF-receptor. Cancer Res 2001;61:2404–8.
13. Leunig M, Yuan F, Menger MD, et al. Angiogenesis, microvascular architecture, microhemodynamics, and intestinal fluid pressure during early growth of human adenocarcinoma LS174T in SCID mice. Cancer Res 1992;52:6553–60.
14. Brown EB, Campbell RB, Tsuzuki Y, et al. In vivo measurement of gene expression, angiogenesis and physiological function in tumors using multiphoton laser scanning microscopy. Nat Med 2001;7:864–8.
15. Padera TP, Stoll BR, So PT, Jain RK. Conventional and high-speed intravital multiphoton laser scanning microscopy of microvasculature, lymphatics, and leukocyte-endothelial interactions. Mol Imaging 2002;1:9–15.
16. Mouta Carreira C, Nasser SM, di Tomaso E, et al. LYVE-1 is not restricted to the lymph vessels: expression in normal liver blood sinusoids and down-regulation in human liver cancer and cirrhosis. Cancer Res 2001;61:8079–84.
17. Padera TP, Stoll BR, Tooredman JB, et al. Cancer cells compress intratumour vessels. Nature (Lond) 2004;427:695.
18. Karpanen T, Egeblad M, Karkkainen MJ, et al. Vascular endothelial growth factor-C promotes tumor lymphangiogenesis and intralymphatic tumor growth. Cancer Res 2001;61:1786–90.
19. Krishnan J, Kirkin V, Steffen A, et al. Differential in vivo and in vitro expression of vascular endothelial growth factor (VEGF)-C and VEGF-D in tumors and its relationship to lymphatic metastasis in immunocompetent rats. Cancer Res 2003;63:713–22.
20. Schmid-Schönbein GW. The second valve system in lymphatics. Lymph Res Biol 2003;1:25–31.
21. Jain RK. Molecular regulation of vessel maturation. Nat Med 2003;9:685–93.

Peritumor Lymphatics Induced by Vascular Endothelial Growth Factor-C Exhibit Abnormal Function

Naohide Isaka, Timothy P. Padera, Jeroen Hagendoorn, et al.

Cancer Res 2004;64:4400-4404.